

# Berry phase of non-ideal Dirac fermions in topological insulators

A. A. Taskin and Yoichi Ando

*Institute of Scientific and Industrial Research, Osaka University, Ibaraki, Osaka 567-0047, Japan*

(Dated: April 7, 2019)

A distinguishing feature of Dirac fermions is the Berry phase of  $\pi$  associated with their cyclotron motions. Since this Berry phase can be experimentally assessed by analyzing the Landau-level fan diagram of the Shubnikov-de Haas (SdH) oscillations, such an analysis is widely employed in recent transport studies of topological insulators to elucidate the Dirac nature of the surface states. However, the reported results have usually been unconvincing. Here we show a general scheme for describing the phase factor of the SdH oscillations in realistic surface states of topological insulators, and demonstrate how one could elucidate the Dirac nature in the real experimental data.

PACS numbers: 73.25.+i, 73.20.At, 71.70.Di, 72.20.My

During the last three decades, the Berry phase<sup>1</sup> has become an important concept in condensed matter physics,<sup>2</sup> playing a fundamental role in various phenomena such as electric polarization, orbital magnetism, anomalous Hall effects, *etc.*<sup>3</sup> The Berry phase (or geometrical phase) in solids is determined by topological characteristics of the energy bands in the Brillouin zone (BZ) and represents a fundamental property of the system. For example, a non-zero Berry phase, which can be measured directly in the magnetotransport experiments, reflects the existence of a singularity in the energy bands such as a band-contact line in three-dimensional (3D) bulk states or a Dirac point in a two-dimensional (2D) surface state.<sup>4</sup> Also, the Berry phase of  $\pi$  is responsible for the peculiar “anti-localization” effects in carbon nanotubes or graphene.<sup>5</sup> Recently, the  $\pi$  Berry phase has been observed in the Shubnikov-de Haas (SdH) oscillations in graphene,<sup>6,7</sup> giving one of the key evidences for the Dirac nature of quasiparticles in the 2D carbon sheet.

The 3D topological insulator (TI) also supports spin polarized 2D Dirac fermions on its surface,<sup>8</sup> which can be distinguished from ordinary charge carriers by a non-zero Berry phase. Recently, several groups have reported observations of the SdH oscillations coming from the 2D surface states of TIs.<sup>9–16</sup> In those studies, a finite Berry phase has been reported, but it usually deviates from the exact  $\pi$  value. For example, in the new TI material Bi<sub>2</sub>Te<sub>2</sub>Se (BTS),<sup>12</sup> where a large contribution of the surface transport to the total conductivity has been observed, the apparent Berry phase extracted from the SdH-oscillation data was  $0.44\pi$ . So far, the Zeeman coupling of the spin to the magnetic field has been considered<sup>11</sup> as a possible source of such a discrepancy. In this Rapid Communication, we show that in addition to the Zeeman term, the deviation of the dispersion relation  $E(k)$  from an ideal linear dispersion<sup>17</sup> can shift the Berry phase from  $\pi$ . We further show how the real experimental data for non-ideal Dirac fermions could be understood by taking into account those additional factors.

The energy dispersion of the surface states in TIs can be directly measured in angle-resolved photoemission spectroscopy (ARPES) experiments. As an example, Fig.

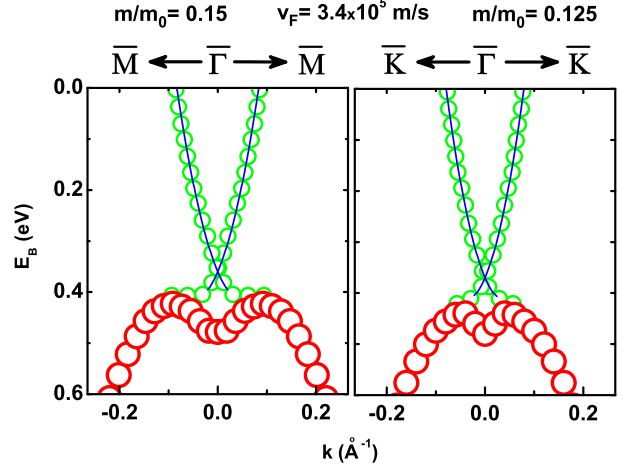


FIG. 1: (Color online) Experimental band dispersions (symbols) in Bi<sub>2</sub>Te<sub>2</sub>Se measured by ARPES in Ref. 18 and the fitting of Eq. (1) to the surface state (solid line). Large symbols depict the bulk state.

1 shows the dispersion of the surface state (together with the bulk state) in BTS reported by Xu *et al.*<sup>18</sup> One can easily recognize that  $E(k)$  is not an ideal Dirac-like dispersion, but it can be fitted reasonably well for the two high-symmetry axes with

$$E(k) = v_F \hbar k + \frac{\hbar^2}{2m} k^2, \quad (1)$$

with a single Fermi velocity  $v_F = 3.4 \times 10^5$  m/s and the effective mass  $m$  which slightly varies with the direction in the surface BZ as shown by the solid lines in Fig. 1 [ $m/m_0 = 0.15$  (0.125) for the  $\bar{\Gamma} \rightarrow \bar{M}$  ( $\bar{\Gamma} \rightarrow \bar{K}$ ) direction with  $m_0$  the free electron mass].

In the SdH oscillations, the oscillating part of  $\rho_{xx}$  follows

$$\Delta \rho_{xx} \sim \cos[2\pi(\frac{F}{B} - \gamma)], \quad (2)$$

where  $F$  is the oscillation frequency and  $2\pi\gamma$  is the phase factor ( $0 \leq \gamma < 1$ ). This is the same  $\gamma$  as in the Onsager’s

quantization condition<sup>19</sup>

$$A_N = \frac{2\pi e}{\hbar} B(N + \gamma), \quad (3)$$

when the  $N$ -th Landau level (LL) is crossing the Fermi energy  $E_F$  ( $A_N$  is the area of an electron orbit in the  $k$ -space).  $\gamma$  is directly related to the Berry phase through<sup>4</sup>

$$\gamma - \frac{1}{2} = -\frac{1}{2\pi} \oint_{\Gamma} \vec{\Omega} d\vec{k}, \quad (4)$$

where  $\vec{\Omega}(\vec{k}) = i \int d\vec{k}' u_{\vec{k}'}^*(\vec{r}) \vec{\nabla}_{\vec{k}'} u_{\vec{k}}(\vec{r})$  is the Berry connection,  $u_{\vec{k}}(\vec{r})$  is the amplitude of the Bloch wave function,  $\Gamma$  is a closed electron orbit (the intersection of the Fermi surface  $E(\vec{k}) = E_F$  with the plane  $k_z = \text{const}$ ). For spinless quasiparticles, it is known<sup>4,19</sup> that the Berry phase is zero for a parabolic energy dispersion ( $\gamma = \frac{1}{2}$ ) and  $\pi$  for a linear energy dispersion ( $\gamma = 0$ ).

Experimentally,  $\gamma$  can be obtained from an analysis of the Landau-level (LL) fan diagram. There are three quantities which are often used as abscissa for plotting a LL fan diagram: (i) Landau level index  $N$ , which determines the energy  $E_N$  of the  $N$ -th LL. (ii) Filling factor  $\nu$  ( $\equiv \frac{N_s S}{N_\phi}$ , where  $N_s$  is the density of charge carriers,  $S$  is the area of the sample,  $N_\phi = \frac{BS}{\Phi_0}$  is the number of flux quanta, and  $\Phi_0 = \frac{h}{e}$  is the flux quantum). (iii) An integer number  $n$  which marks the  $n$ -th minimum of the oscillations in  $\rho_{xx}$ . Although all three quantities are related to each other, the most straightforward way to plot a LL fan diagram from the  $\rho_{xx}$  oscillations in a 2D system<sup>9</sup> is to assign an integer  $n$  to a minimum of  $\rho_{xx}$  (or a half-integer to a maximum of  $\rho_{xx}$ ). From Eq. (2), one can see that the first minimum in  $\rho_{xx}$  is always in the range of  $0 < \frac{F}{B_1} \leq 1$ . Thus, the plot of  $F/B_n$  vs.  $n$ , which makes a straight line with a unit slope for periodic oscillations, is uniquely defined and cuts the  $n$ -axis between 0 and 1 depending on the phase of the oscillations,  $\gamma$ .

The ordinate  $1/B_n$  in a LL fan diagram is determined by the Landau quantization of the cyclotron motion of electrons in a magnetic field. In 2D systems, upon sweeping  $B$ ,  $\rho_{xx}$  shows a maximum (or a sharp peak in the quantum Hall effect<sup>9</sup>) each time when  $E_N(B)$  crosses the Fermi level. Thus, the position of the maximum in  $\rho_{xx}$  that corresponds to the  $N$ -th LL,  $1/B_N$ , is given by

$$2\pi \left( \frac{F}{B_N} - \gamma \right) = 2\pi N. \quad (5)$$

On the other hand, the  $n$ -th minimum in  $\rho_{xx}$  occurs at  $1/B_n$  when  $2\pi \left( \frac{F}{B_n} - \gamma \right) = 2\pi n - \pi$ , so the positions of the maxima and minima are shifted by  $\frac{1}{2}$  on the  $n$ -axis.

The Onsager's relation<sup>19</sup> gives  $F$  in terms of the Fermi wave vector  $k_F$  as  $F = (\hbar/2\pi e)\pi k_F^2$ , and this  $k_F$  can be calculated from Eq. (1) as

$$k_F^2 = 2 \left( \frac{mv_F}{\hbar} \right)^2 \left( 1 + \frac{E_F}{mv_F^2} - \sqrt{1 + \frac{2E_F}{mv_F^2}} \right). \quad (6)$$

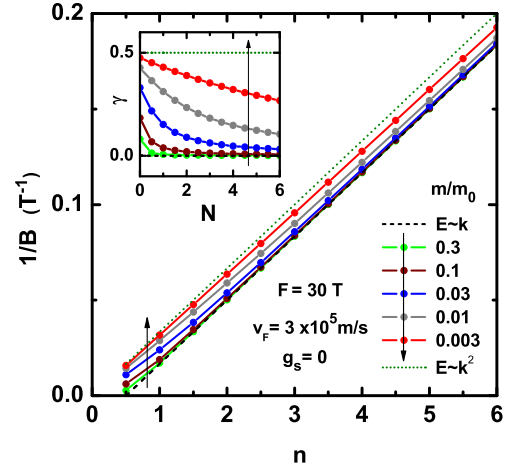


FIG. 2: (Color online) Landau level fan diagram calculated for  $F = 30$  T,  $v_F = 3 \times 10^5$  m/s,  $g_s = 0$ , and different  $m/m_0$ . Arrows show the direction of decreasing  $m/m_0$ . The dashed and dotted lines are the expected behaviors for an ideal Dirac dispersion and a parabolic dispersion, respectively. Inset shows the calculated  $\gamma(N)$ .

Also, when  $E_F$  is at the  $N$ -th LL, there is a relation

$$E_N(B_N) = E_F. \quad (7)$$

From Eqs. (5)–(7), one obtains

$$\gamma = \frac{mv_F^2}{\hbar \omega_c} \left( 1 + \frac{E_N}{mv_F^2} - \sqrt{1 + \frac{2E_N}{mv_F^2}} \right) - N, \quad (8)$$

where  $\omega_c = eB/m$  is the cyclotron frequency.

In two extreme cases, Eq. (8) gives the expected results. First, for a linear dispersion,  $m \rightarrow \infty$  leads to  $\gamma \rightarrow \frac{E_N^2}{2\hbar e v_F^2 B} - N$ , where  $E_N = \pm \sqrt{2\hbar e v_F^2 B N}$ , giving  $\gamma = 0$ . Second, for a parabolic dispersion,  $v_F \rightarrow 0$  leads to  $\gamma \rightarrow \frac{E_N}{\hbar \omega_c} - N$ , where  $E_N = \hbar \omega_c (N + \frac{1}{2})$ , giving  $\gamma = \frac{1}{2}$ . This gives confidence that the expression for  $\gamma$  given in Eq. (8) is generally valid for the topological surface state with a non-ideal Dirac cone described by Eq. (1). In a general case, however,  $\gamma$  is actually a function of  $B$  and oscillations in  $\rho_{xx}$  are only quasi-periodic in  $1/B$ . Nevertheless, if the series of eigenvalues  $E_N$  for a given Hamiltonian is known, the positions of maxima (and hence minima) in  $\rho_{xx}$  can be found from Eq. (5) using Eq. (8).

For the (111) surface state of the  $\text{Bi}_2\text{Se}_3$ -family TI compounds, the Hamiltonian for non-ideal Dirac quasiparticles in perpendicular magnetic fields can be written as<sup>20</sup>

$$\hat{H} = v_F (\Pi_x \sigma_y - \Pi_y \sigma_x) + \frac{\Pi^2}{2m} - \frac{1}{2} g_s \mu_B B \sigma_z, \quad (9)$$

where the Landau gauge  $\mathbf{A} = (0, By, 0)$  for the vector potential is used,  $\Pi = \hbar \mathbf{k} + e\mathbf{A}$ ,  $\sigma_i$  are the Pauli matrices,  $\mu_B$  is the Bohr magneton, and  $g_s$  is the surface  $g$ -factor.

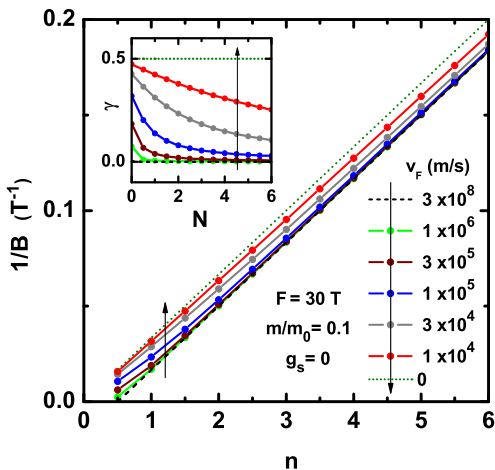


FIG. 3: (Color online) Landau level fan diagram calculated for  $F = 30$  T,  $m/m_0 = 0.1$ ,  $g_s = 0$ , and different  $v_F$ . Arrows show the direction of decreasing  $v_F$ . Inset shows calculated  $\gamma(N)$ .

The LL energies are given by<sup>20</sup>

$$E_N^{(\pm)} = \hbar\omega_c N \pm \sqrt{2\hbar v_F^2 eBN + \left(\frac{1}{2}\hbar\omega_c - \frac{1}{2}g_s\mu_B B\right)^2}, \quad (10)$$

where “+” and “-” branches are for electrons and holes, respectively.

Let us first consider how the LL fan diagram will be modified, when both linear and parabolic terms are present in the Hamiltonian [Eq. (9)]. For the moment, the Zeeman coupling of the electron spin to the magnetic field is assumed to be negligible ( $g_s = 0$ ). Figure 2 shows the calculated positions of maxima and minima in  $\rho_{xx}$  for oscillations with  $F = 30$  T and  $v_F = 3 \times 10^5$  m/s as  $m/m_0$  is varied. One can see that upon decreasing  $m/m_0$ , the calculated lines on the LL fan diagram are gradually shifting upward from the ideal Dirac line that crosses the  $n$ -axis at exactly  $\frac{1}{2}$ . Moreover, the lines are not straight anymore, which is clearly inferred in the dependence of  $\gamma$  vs  $N$  shown in the inset. With decreasing  $N$  (increasing  $B$ ),  $\gamma$  becomes larger, reflecting the change in the phase of oscillations at high fields.

Similar change in the LL fan diagram occurs if we modify another parameter,  $v_F$ . As shown in Fig. 3, the calculated lines are gradually shifting upward from the ideal Dirac line as  $v_F$  is decreased. The results shown in Figs. 2 and 3 can be understood as a competition between linear and quadratic terms in the Hamiltonian [Eq. (9)]. Note that for the whole range of the parameters  $v_F$  and  $m/m_0$ , the positions of maxima and minima in  $\rho_{xx}$  lie between two straight lines (shown as dotted and dashed lines in Figs. 2 and 3) corresponding to  $\gamma = 0$  and  $\gamma = \frac{1}{2}$ .

Let us now take the Zeeman term into considerations. Figure 4 shows the LL fan diagram calculated with  $F = 30$  T,  $v_F = 3 \times 10^5$  m/s, and  $m/m_0 = 0.1$ , while  $g_s$  is varied. To understand the effect of the Zeeman coupling,

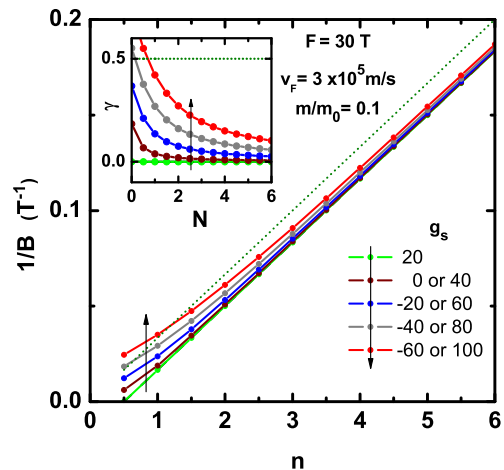


FIG. 4: (Color online) Landau level fan diagram calculated for  $F = 30$  T and different  $g_s$ , keeping  $v_F = 3 \times 10^5$  m/s and  $m/m_0 = 0.1$  constant. Arrows show the direction of changing  $g_s$ . The dashed line is the expected behaviors for a parabolic dispersion, Inset shows calculated  $\gamma(N)$ .

it is important to recognize the following two points: (i) The Zeeman term in Eq. (10) would tend to cancel the  $\frac{1}{2}\hbar\omega_c$  term when  $g_s$  is positive. In fact, when  $\frac{1}{2}\hbar\omega_c = \frac{1}{2}g_s\mu_B B$  (*i.e.*,  $g_s = 2m_0/m$ ) is satisfied, the effect of the finite effective mass is canceled and the LL fan diagram becomes identical to that for the linear dispersion (ideal Dirac) case. In the present simulations, we use  $m/m_0 = 0.1$ , so that this cancellations occurs when  $g_s = 20$ . (ii) A pair of  $g_s$  values that give the same  $|\frac{1}{2}\hbar\omega_c - \frac{1}{2}g_s\mu_B B|$  are effectively the same in determining the behavior of the LL fan diagram. The result of our calculations shown in Fig. 4 is a demonstration of these two points. Since the Zeeman effect is more pronounced at higher fields, the LL fan diagram in Fig. 4 is strongly modified from a straight line when the quantum limit is approached, *i.e.*, close to  $N = 0$ .

Finally, let us examine the real data measured in the BTS sample,<sup>12</sup> in the light of the above considerations. Figure 5 shows the LL fan diagram for oscillations in  $d\rho_{xx}/dB$  measured at  $T = 1.6$  K in magnetic fields perpendicular to the (111) plane.<sup>12</sup> In Ref. 12, the data were simply fitted with a straight line, and the least-square fitting gave a slope of  $F = 64$  T with the intersection of the  $n$ -axis at  $0.22 \pm 0.12$ ; this result implies a finite Berry phase, but it was not exactly equal to  $\pi$ , which remained a puzzle.<sup>12</sup> Now, we analyze this LL fan diagram by considering the non-ideal Dirac dispersion as well as the Zeeman effect. The ARPES data<sup>18</sup> for the surface state of BTS (Fig. 1) gives  $v_F = 3.4 \times 10^5$  m/s and the averaged effective mass  $m/m_0 = 0.13$ . We fix the oscillation frequency  $F$  at 62 T obtained from the Fourier-transform analysis of the  $d\rho_{xx}/dB$  oscillations.<sup>12</sup> In Fig. 5, the calculated diagram for an ideal Dirac cone is shown by the thin (orange) solid line, whereas that for the non-ideal Dirac cone with the effective-mass term is shown by the

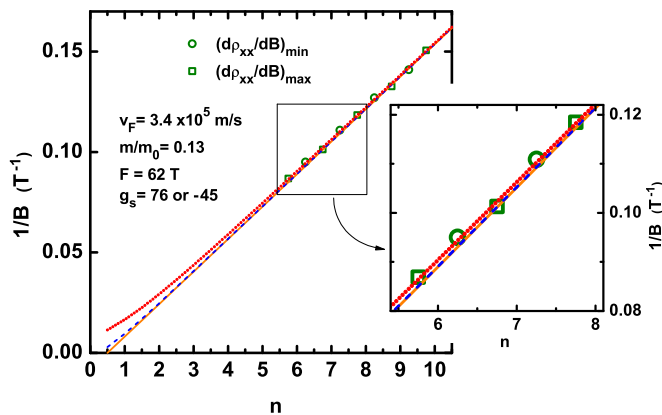


FIG. 5: (Color online) Landau level fan diagram for oscillations in  $d\rho_{xx}/dB$  measured at  $T = 1.6$  K and  $\theta \simeq 0^\circ$  reported in Ref. 12 for BTS. Minima and maxima in  $d\rho_{xx}/dB$  correspond to  $n + \frac{1}{4}$  and  $n + \frac{3}{4}$ , respectively. Solid (orange) line is the calculated diagram for an ideal Dirac cone with  $v_F = 3.4 \times 10^5$  m/s and  $F = 62$  T; dashed (blue) line includes the effect of the actual dispersion with  $m/m_0 = 0.13$ ; dotted (red) line further includes the Zeeman effect, where  $g_s = 76$  or  $-45$  was determined from a least-square fitting to the data. Inset shows a magnified view of the fitting for smaller  $n$ .

dashed (blue) line. One can see that the difference is small, which indicates that the effective mass of  $0.13m_0$  is not light enough to significantly alter the LL fan diagram. One may also see that these two lines undershoot the actual data points at smaller  $n$ . However, by further

including the Zeeman effect, we can greatly improve the analysis, as shown by the dotted (red) line; here,  $g_s$  is taken as the only fitting parameter and a least-square fitting to the data was performed. The best value of  $g_s$  is 76 or  $-45$ , and the former is similar to that reported<sup>11</sup> for the surface state of  $\text{Bi}_2\text{Se}_3$  and is not unreasonable for a narrow-gap semiconductor. Therefore, one may conclude that an advanced analysis considering both the curvature of the Dirac cone and the Zeeman effect can reasonably describe the data of the LL fan diagram, confirming the Dirac nature in the surface state of BTS.

In summary, we derived the formula for the phase of the SdH oscillations coming from the surface Dirac fermions of realistic topological insulators with a non-ideal dispersion given by Eq. (1). We also calculated how the curvature in the dispersion as well as the effect of Zeeman coupling affect the Landau-level fan diagram of the SdH oscillations for realistic parameters. Finally, we demonstrate that the Landau-level fan diagram recently reported for the surface SdH oscillations in  $\text{Bi}_2\text{Te}_2\text{Se}$ , which suggested an intermediate value of the Berry phase in a simple analysis, can actually be understood to signify a relatively large Zeeman effect.

We thank G.P. Mikitik for helpful discussions. This work was supported by JSPS (KAKENHI 19674002 and the Next-Generation World-Leading Researchers Program), MEXT (Innovative Area “Topological Quantum Phenomena” KAKENHI 22103004), and AFOSR (AOARD 10-4103).

<sup>1</sup> M.V. Berry, Proc. R. Soc. London A **392**, 45 (1984).  
<sup>2</sup> A. Shapere and F. Wilczek, *Geometrical Phase in Physics* (World Scientific, Singapore, 1989).  
<sup>3</sup> D. Xiao, M.C. Chang, and Q. Niu, Rev. Mod. Phys. **82**, 1957 (2010).  
<sup>4</sup> G.P. Mikitik and Yu.V. Sharlai, Phys. Rev. Lett. **82**, 2147 (1999).  
<sup>5</sup> T. Ando, T. Nakanishi, and R. Saito, J. Phys. Soc. Jpn. **67**, 2857 (1998).  
<sup>6</sup> K.S. Novoselov, A.K. Geim, S.V. Morozov, D. Jiang, M.I. Katsnelson, I.V. Grigorieva, S.V. Dubonos, and A.A. Firsov, Nature (London) **438**, 197 (2005).  
<sup>7</sup> Y. Zhang, Y.-W. Tan, H.L. Stormer, and P. Kim, Nature (London) **438**, 201 (2005).  
<sup>8</sup> M.Z. Hasan and C.L. Kane, Rev. Mod. Phys. **82**, 3045 (2010).  
<sup>9</sup> D.-X. Qu, Y.S. Hor, J. Xiong, R.J. Cava and N.P. Ong, Science **329**, 821 (2010).  
<sup>10</sup> A.A. Taskin, K. Segawa, and Y. Ando, Phys. Rev. B **82**, 121302(R) (2010).  
<sup>11</sup> J.G. Analytis, R.D. McDonald, S.C. Riggs, J.-H. Chu, G.S. Boebinger, and I.R. Fisher, Nat. Phys. **10**, 960-964 (2010).  
<sup>12</sup> Z. Ren, A.A. Taskin, S. Sasaki, K. Segawa, and Y. Ando,

Phys. Rev. B **82**, 241306(R) (2010).  
<sup>13</sup> J. Xiong, A.C. Petersen, Dongxia Qu, R. J. Cava, and N. P. Ong, arXiv:1101.1315.  
<sup>14</sup> B. Sacépé, J.B. Oostinga, J. Li, A. Ubalini, N.J.G. Couto, E. Giannini, and A.F. Morpurgo, arXiv:1101.2352.  
<sup>15</sup> C. Brüne, C.X. Liu, E.G. Novik, E.M. Hankiewicz, H. Buhmann, Y.L. Chen, X.L. Qi, Z.X. Shen, S.C. Zhang, L.W. Molenkamp, arXiv:1101.2627.  
<sup>16</sup> F. Xiu, L. He, Y. Wang, L. Cheng, L.-T. Chang, M. Lang, G. Huang, X. Kou, Y. Zhou, X. Jiang, Z. Chen, J. Zou, A. Shailos, and K.L. Wang, Nat. Nano. doi:10.1038/nnano.2011.19.  
<sup>17</sup> D. Culcer, E.H. Hwang, T.D. Stanescu, and S. Das Sarma, Phys. Rev. B **82**, 155457 (2010).  
<sup>18</sup> S.Y. Xu, L.A. Wray, Y. Xia, R. Shankar, A. Petersen, A. Fedorov, H. Lin, A. Bansil, Y.S. Hor, D. Grauer, R.J. Cava, and M.Z. Hasan, arXiv:1007.5111v1.  
<sup>19</sup> D. Shoenberg, *Magnetic Oscillations in Metals* (Cambridge University Press, Cambridge, 1984).  
<sup>20</sup> Z. Wang, Z.-G. Fu, S.-X. Wang, and P. Zhang, Phys. Rev. B **82**, 085429 (2010).